ORIGINAL PAPER

High Temperature Corrosion of HVOF Coatings in Laboratory-Simulated Biomass Combustion Superheater Environments

Andy Pidcock[1] · Stefano Mori[2] · Joy Sumner[2] · Nigel Simms[2] · John Nicholls[2] · John Oakey[2]

Abstract

This study examines the fireside corrosion of FeCrAl, NiCr, NiCrAlY and A625 coatings applied by 'high velocity oxy fuel'(HVOF) and exposed to simulated biomass firing conditions (gas composition CO_2, N_2, SO_2 and HCl). The coatings and a typical base steel alloy (T92) were exposed to simulated conditions at 600 °C for 1000 h in a laboratory scale furnace. Samples were coated with a potassium chloride deposit. Samples were then cold mounted in a low-shrinkage epoxy resin and then cross-sectioned. Corrosion was assessed by dimensional metrology comparing the coating thickness change of the samples. The cross-sections of the 'worst' and 'best' coatings were examined. Results show that all but one coating (HVOF NiCr) outperformed the T92 alloy. No coating composition or method was conclusively better. Evidence of Cr depletion as well as the formation of a sulphidation layer have been found in the exposed samples with coatings. The formation of a K_2SO_4 layer has also been observed on all coated specimens.

Keywords Metal coatings · Molten salts · High temperature corrosion · Fireside corrosion

Introduction

The European Union (EU) and the United Kingdom (UK), through the UK Climate Change Act 2008, have set targets for a net 80% reduction in greenhouse gas (GHG) emissions by 2050 against a 1990 baseline [1–3]. The EU's 2030 climate and energy package has proposed an intermediate target of a 40% net reduction in GHG emissions by 2030 [3–5]. Achievement of such reductions is believed to be impossible without a

✉ Stefano Mori
  stefano.mori@cranfield.ac.uk

Extended author information available on the last page of the article

95–100% decarbonisation of the power sector, and studies have looked at three parallel pathways for achieving this: fossil fuel plus carbon capture and storage (CCS); nuclear energy; a mix of renewable technologies [1]. Energy generated through the combustion of biomass fuels is considered renewable, and this is currently the EU's biggest source of renewable energy [6].

Solid fuel fired power generation systems operate within the context of competing environmental, technical, regulatory and economic pressures. The co-combustion of biomass in coal-fired plant was the first step into large scale energy production [7–9]. However, legislative frameworks are placing ever stricter limits on SO_x, NO_x, and CO_2 emissions, and systems fired on biomass alone are being encouraged by regulatory actions in some countries to meet CO_2 reduction targets [10–15].

For combustion plant firing biomass alone, the superheaters and reheaters experience deposit compositions that can be richer in chlorides than coal-fired systems due to the higher Cl/S ratio of biomass fuels [16, 17]. These deposits produce more corrosive environments on the superheaters/reheaters [18–23]. As a result, to maintain components lives, most biomass plants use lower steam temperatures (and pressures), and hence achieve lower energy conversion efficiencies [24]. An alternative approach to lowering steam temperatures would be to use, or develop, more corrosion-resistant materials e.g., Ni-based alloys or new stainless steels. However, existing advanced alloys are expensive and alloy development takes a long time (10–20 years). Coatings offer a more immediate solution to improving the performance of the surface of existing materials, for example a cheaper stainless-steel coating on T92. If coatings are to be adopted, as well as resisting corrosion, they must be robust, easy to apply, repairable and cost effective.

In the literature, different coatings have been investigated [25–27]. Some coatings compositions showed promising results for biomass exposure at 600 °C (temperature at which biomass power plants are anticipated to operate) for 72 h using Ni–Al based coatings [27]. The exposure time used under in the study could provide good basis for the characterization of the early stages of the corrosion mechanism but would be insufficient to provide a robust prediction of the longer-term effect. Other studies have pushed to higher temperature (800 °C) but in co-firing simulated environments [25]. As highlighted in several studies, co-firing conditions could produce very different results from pure biomass combustion environment [28, 29]. Furthermore, the degradation mechanisms experienced by some commercially available coatings (e.g., NiCrAlY, alloy 625, Cr_3C_2 in Ni–Cr matrix, FeCrAl, alloy 276 and Ni-50Cr) have been investigated in real coal combustion exposure conditions [30]. Therefore, a better understanding of the degradation processes due to the change in fuel is needed. This paper focuses on the fireside corrosion behaviour of commercially available coatings' chemistry on T92 substrate in simulated biomass post-combustion environment.

Experimental Procedures

Materials and Coatings

Base alloy specimens were pre-prepared prior to coating and sectioning into individual samples. The T92 alloy was in the form of a machined string of 'bobbins' (Fig. 1). All surfaces were ground to a P1200 finish prior to coating. Nominal composition of the base alloy is given in Table 1. Four candidate coatings (FeCrAl, NiCr, NiCrAlY and A625) were applied to the base alloy using a JP5000 HVOF (high velocity oxy fuel) system at Monitor Coatings. The nominal compositions of the HVOF powders are given in Table 2. The powders were sourced from Sulzer Metco. After coating the specimens were cut into individual samples using a metallographic cut-off saw.
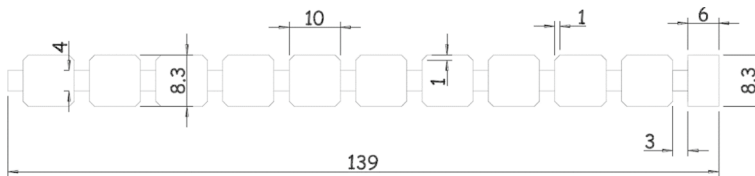

Fig. 1 Design drawing for string of T92 'bobbin' samples (all dimensions in mm)

Table 1 ASTM A213 composition specification of T92 (wt%) [31]

Alloy	C	Si	Cr	Fe	Ni	Mn	Mo	W	Other
T92	0.07–0.13	<0.50	8.5–9.5	Bal	<0.40	0.30–0.60	0.30–0.60	1.5–2.00	B (0.001–0.006) N (0.030–0.070), Al (<0.02) P (<0.020), S (<0.010) Ti (<0.01), V (0.15–0.25) Zr (<0.01), Nb (0.04–0.09)

Table 2 Composition specifications HVOF spray powders (wt%)

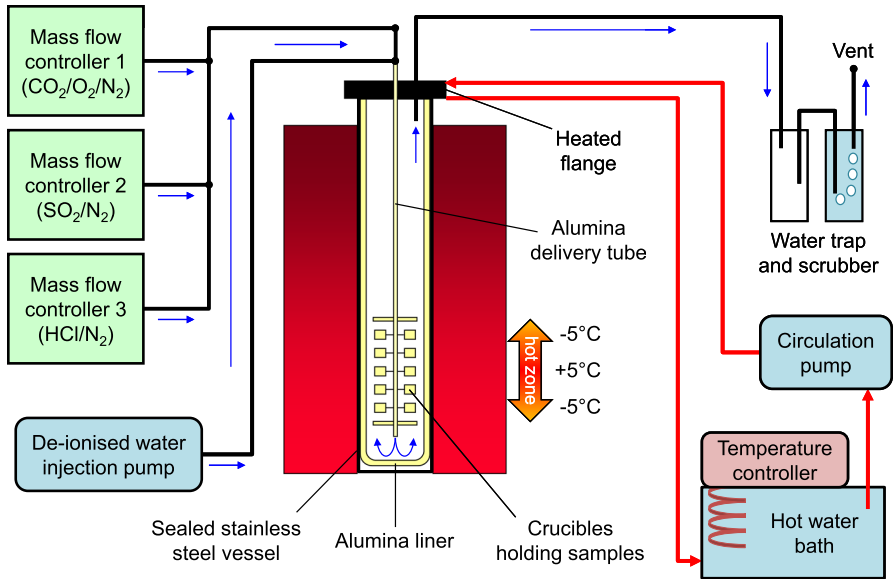| Coating	Al	Si	Cr	Fe	Ni	Nb+Ta	Mo	Other
FeCrAl	5.9	0.83	21.7	Bal	–	–	–	C (0.03), P (0.01) S (0.01), Mn (0.75)
NiCr	–	2.1	46.0	1.1	Bal	–	–	C (0.1), O (0.03)
NiCrAlY	9.9	–	22.0	–	Bal	–	–	O (0.02), Y (0.9)
A625	0.2	0.13	21.3	0.1	Bal	3.58	8.9	N (0.03), Co (0.1) Cu (0.18)

Fig. 2 Schematic diagram of the controlled atmosphere furnace [25, 32, 33]

Table 3 Gas mixtures used in controlled atmosphere furnace

Environment	Fuel Mix [wt%]	CO_2 [vol%]	O_2 [vol%]	N_2 [vol%]	SO_2 [vppm]	HCl [vppm]	H_2O [vol%]
Biomass	100% CCP	12.6	4	Bal	240	90	13.5

Corrosion Exposures

Fireside combustion conditions were simulated using an established 'deposit recoat' technique and the injection of pre-mixed bottled gases into an alumina-lined vertical tube furnace (Fig. 2) [25, 28, 29, 32, 33]. All exposures were conducted at 600 °C for 1000 h (five 200 h cycles), with samples of each alloy/coating combination exposed to biomass conditions. Gas mix compositions is given in Table 3, and were simplified in line with other studies assuming that CO_2, N_2, SO_2 and HCl were respectively the only carbon, nitrogen, sulphur and chlorine containing species in the inlet gases [32, 34]. Deposits were applied before first exposure and at subsequent 200 h intervals by mixing with an iso-propyl alcohol carrier and brushing evenly across each sample (on the main body of bobbins). Deposit fluxes range between 50 and 200 μg/cm^2/h. This technique has been widely used in the literature and provides an efficient tool for understanding the corrosion mechanisms taking place under different exposure conditions [28, 29, 33–36]. These types of test are performed under accelerated conditions as per standard [37].

The mass of each sample was recorded, initially and at each 200 h cycle using a Sartorius CP225D five place balance, to ensure consistent deposit fluxes and to monitor changes associated with corrosion. Mass data were interpreted by assuming changes were only associated with areas on which deposit was applied. Gross mass change has been defined as the cumulative mass change (per unit area) of the crucible and its contents, while net mass change is the cumulative mass change (per unit area) of the sample only. In both cases, the mass of deposit applied at each cycle has been subtracted, such that only changes associated with processes occurring during an exposure cycle are presented.

Analysis Techniques

Prior to commencing the corrosion exposures, the test samples were measured using a micrometer (± 1 μm resolution, ± 2 μm accuracy). On completion of the exposures each sample was mounted in epoxy resin mixed with glass ballotini beads (to reduce shrinkage) then cross-sectioned and polished. Separate un-exposed reference samples of each type were also measured and cross-sectioned in the same manner. Non-aqueous methods were used throughout to ensure any deposit/corrosion products were retained. Sectioned samples were then measured using an established technique that utilises a computer controlled semi-automated optical microscope/image analyser system [25, 32, 38].

Image analyser measurements of un-exposed reference samples serve two functions; they provide information on the thickness of the applied coatings, and they allow error due to surface roughness to be accounted for. This comes about because samples that will be exposed can only be measured using a surface contact micrometer, meaning all measurements are at peaks on the surfaces. This error is accounted for by comparing micrometer and image analyser measurements of un-exposed reference samples, and assuming that the systematic difference is representative of all equivalent samples. Pre-exposure micrometer measurements can consequently be 'converted' to more accurately represent the samples. These measurements were subsequently compared with the post-exposure image analyser results to determine metal loss and internal damage distributions around each exposed sample. In this work 'metal loss' (or 'coating loss') and 'sound metal loss' (or 'sound coating loss') are used to compare behaviours; these terms are defined in [39]. The technique has been widely used in the literature and regulated by standard [28, 29, 32–34, 36, 37, 40–42]. A selection of cross-sections of coated samples was also characterised using an FEI XL30 scanning field emission gun (SFEG) and energy dispersive X-ray (EDX) system (Oxford Instruments AztecEnergy V2.2 and AztecHKL V2.2 software).

Results and Discussion

Dimensional Metrology

Simulated Biomass Exposures

Loss distribution plots (Figs. 3 and 4) show the spread of damage measured on each of the exposed coated specimens. The greatest metal losses were recorded for NiCr coatings. Coating failure is considered to have occurred where metal losses are equivalent to the reference coating thicknesses, and this was observed on a significant proportion (~65%) of the sample. The remainder of the NiCr coating on T92 also exhibited a high degree of internal damage.

The same was not observed for NiCrAlY coated T92, which exhibited a uniform metal loss distribution (41 μm median, 78 μm maximum) and a localised region of internal damage; indicated by the peak below 10% on the sound metal loss plot Fig. 3.

The A625 coating exhibited comparable behaviour to substrate alloy, with median metal losses for T92 81 μm (100 μm maximum) and negligible internal damage. The flat distributions in Fig. 3 indicate uniform corrosion across the surface, and there are no regions of complete coating failure.

The lowest median metal loss values were recorded for FeCrAl; −6 μm (49 μm maximum) on T92. Negative values are attributed to damage being very low, meaning it falls within the bounds of measurement error and normal variation in coating thickness. For FeCrAl coated T92, which does not exhibit any internal attack, it can be argued that there has been no corrosion damage on ~95% of the surface, and some localised (but limited) damage on the remainder. Overall, the FeCrAl coating
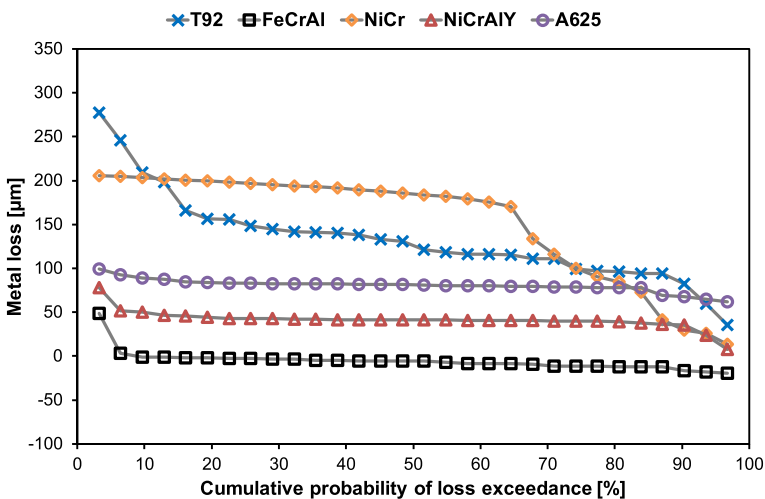

Fig. 3 Metal loss distributions for bare and HVOF coated T92 samples exposed to a simulated biomass environment at 600 °C
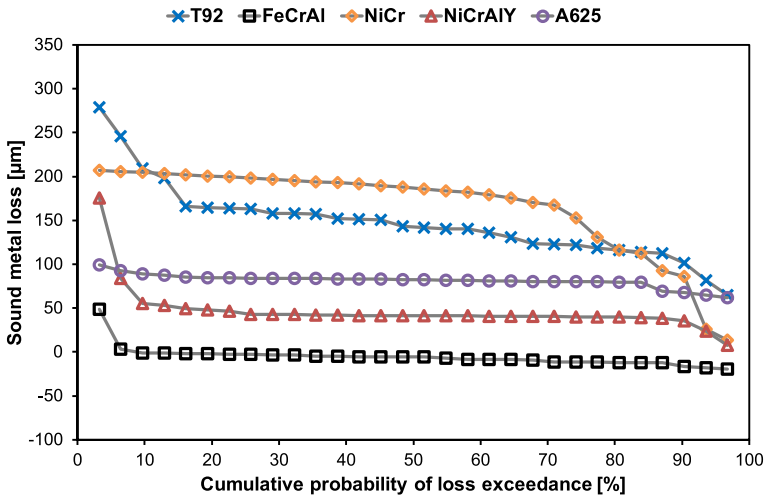
Fig. 4 Sound metal loss distributions for bare and HVOF coated T92 samples exposed to a simulated biomass environment at 600 °C

confers signification improvements over the substrate alloy, although there is a concern with regards the occurrence of local internal attack.

Microscopy Analysis

Unexposed Coatings

Backscatter electron (BSE) images in Fig. 5 show cross-sections through unexposed reference samples of coated T92. All coatings are uniform in thickness, exhibit distinctive 'splat boundaries', with the substrate/coating interfaces characterised by darker regions of voids. Energy dispersive X-ray (EDX) analysis in Table 4 shows that, apart from the slightly elevated chromium and aluminium content of FeCrAl, the compositions of the coatings are consistent with original spray powder specifications.

Exposed Coatings

A BSE image and EDX maps of a representative cross-section through the exposed FeCrAl coated T92 are shown in Fig. 6. The outer surface is characterised by a potassium sulphate layer, which contains small amounts of aluminium, chromium, and iron in proportions different to that of the applied coating. The potassium sulphate is likely associated with the sulphation of the applied potassium chloride deposit in the combustion gases; no chlorine was found in this layer or elsewhere in the cross-section [19–21, 23, 43]. A thin layer of segregated aluminium is observed at the interface with the coating. Both the remaining coating and the substrate appear unaffected compared to the reference sample condition (compare Figs. 5 and 6).
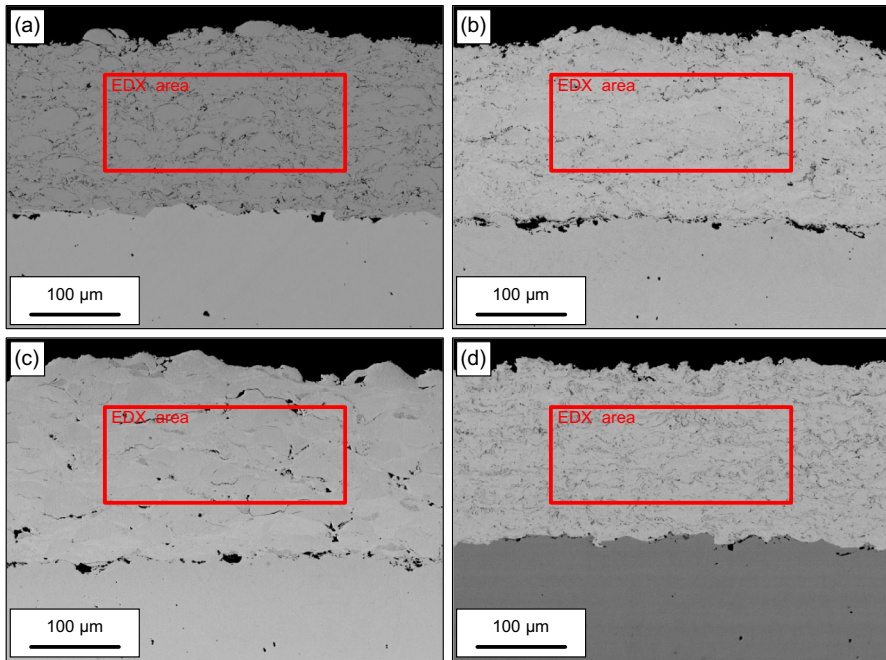
Fig. 5 BSE images and EDX analysis areas of cross-sections through unexposed reference samples of coated T92: **a** FeCrAl, **b** NiCr, **c** NiCrAlY, **d** A625

Table 4 EDX analysis of coating cross-sections shown in Fig. 5 (wt%). Original powder compositions are given in brackets (*specification lists Nb + Ta)

Coating	Al	Si	Cr	Mn	Fe	Ni	Nb	Mo
Figure 5(a) FeCrAl	8.2	–	24.9	–	66.9	–	–	–
	(5.9)	(0.83)	(21.7)	(0.75)	(Bal.)	(–)	(–)	(–)
Figure 5(b) NiCr	–	2.2	47.2	–	–	50.6	–	–
	(–)	(2.1)	(46.0)	(–)	(1.1)	(Bal.)	(–)	(–)
Figure 5(c) NiCrAlY	9.0	–	22.8	–	–	68.2	–	–
	(9.9)	(–)	(22.0)	(–)	(–)	(Bal.)	(–)	(–)
Figure 5(d) A625	–	–	21.4	–	–	66.7	3.5	8.4
	(0.2)	(0.13)	(21.3)	(–)	(0.1)	(Bal.)	(3.58*)	(8.9)

Figure 7 shows a BSE image and EDX maps of a typical region of A625-coated. A thin potassium sulphate layer is visible, followed by a Ni-rich outer oxide, a Cr-rich inner oxide, and a sulphidation layer. The remaining coating and the substrate are unchanged.

A cross-section image and EDX maps of exposed NiCrAlY-coated T92 are shown in Fig. 8. An outer layer of potassium sulphate is again observed, followed by incoherent bands of Ni-rich and Cr-rich oxides. As with the FeCrAl coating, there is
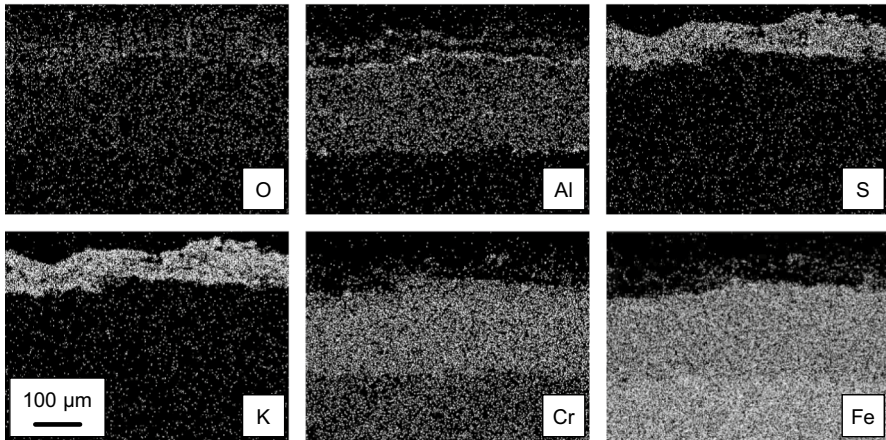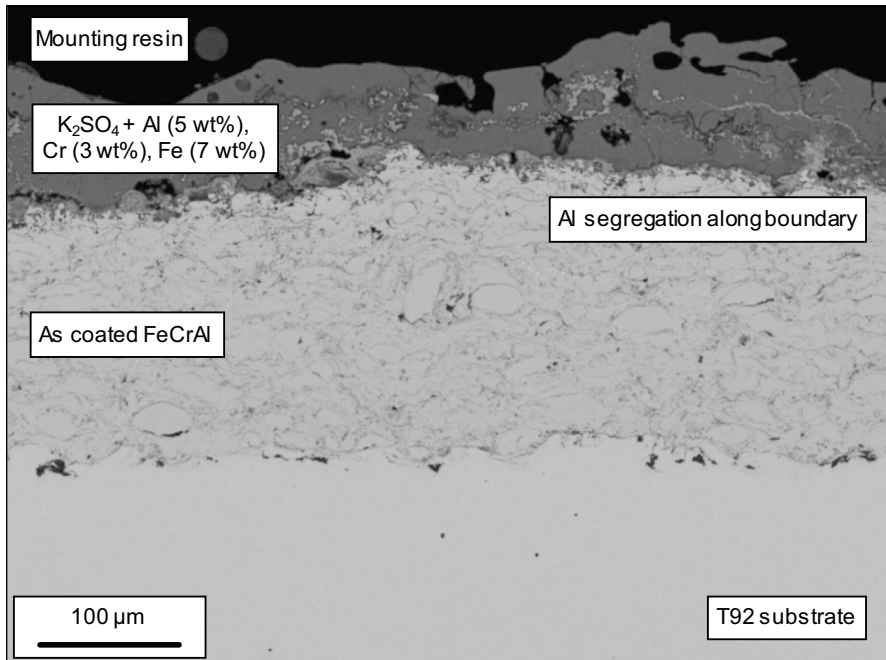
Mounting resin

K_2SO_4 + Al (5 wt%), Cr (3 wt%), Fe (7 wt%)

Al segregation along boundary

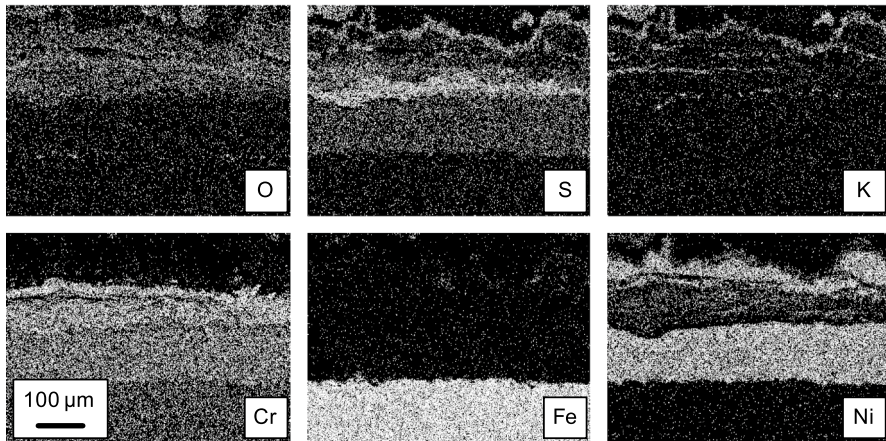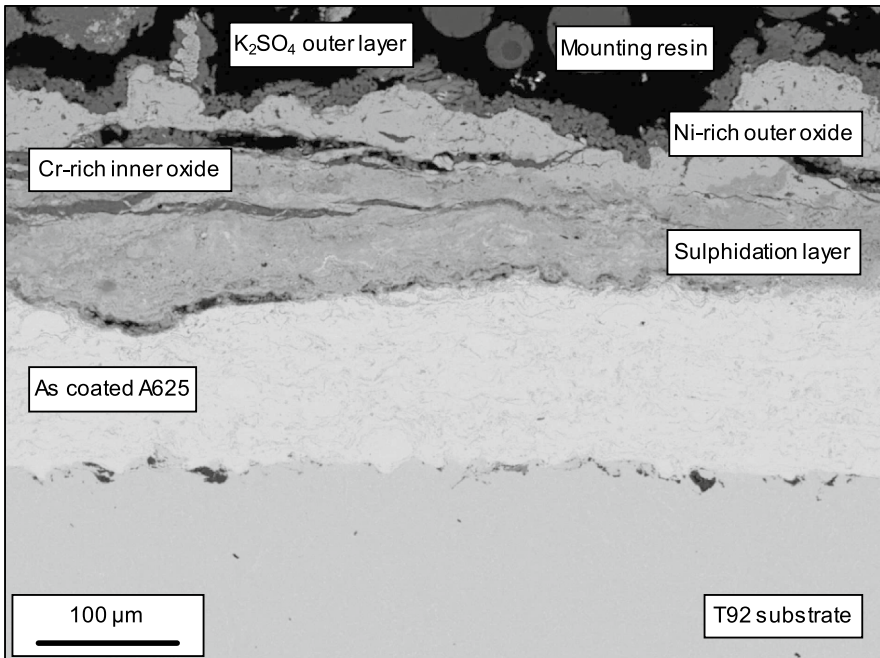As coated FeCrAl

100 μm

T92 substrate

O

Al

S

100 μm

K

Cr

Fe

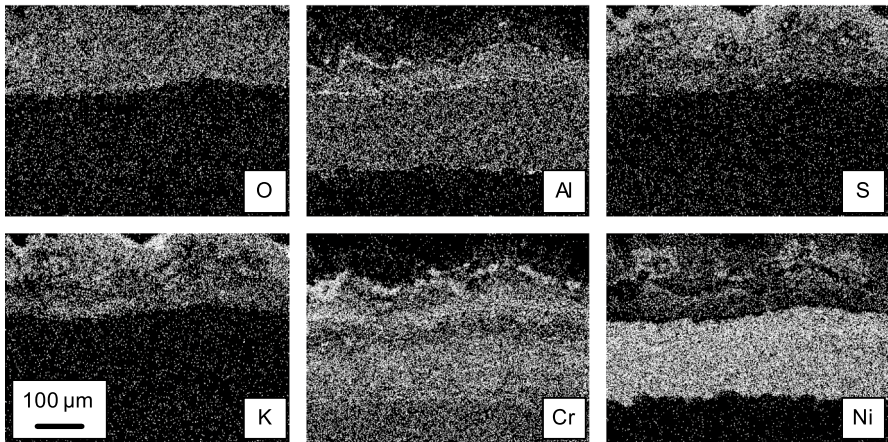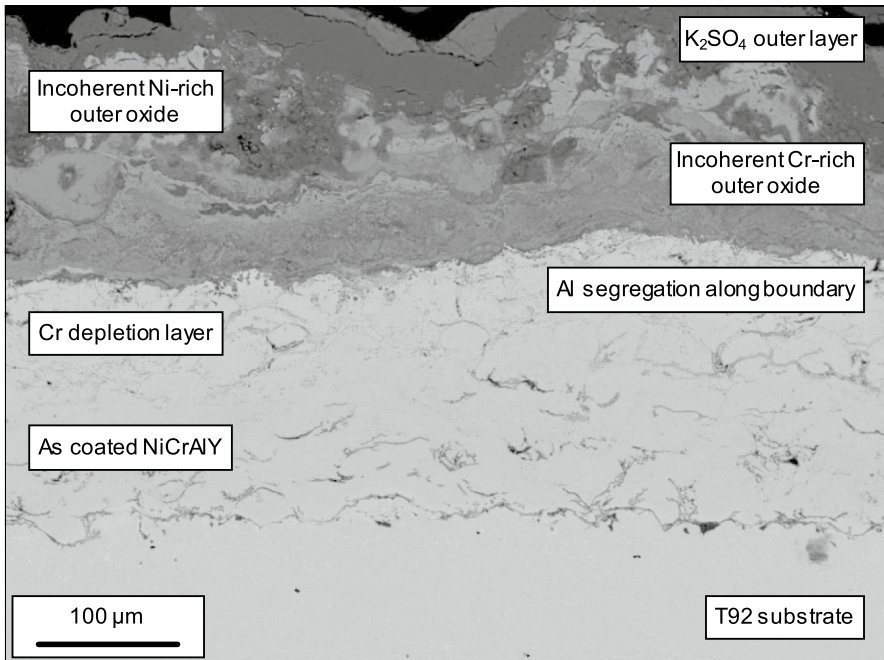**Fig. 6** BSE cross-section image and EDX maps of FeCrAl-coated T92 exposed to a simulated biomass environment at 600 °C for 1000 h

a thin band of segregated Al at the interface with the remaining coating. Within the coating there is also a chromium depleted layer above a band of unaffected coating and the substrate.

Figure 9 shows a BSE cross-section image and EDX maps of exposed NiCr coated T92; noting that the majority of the coating on this sample was lost and this is an atypical region, where some coating remained. A characteristic outer layer of

Fig. 7 BSE cross-section image and EDX maps of A625-coated T92 exposed to a simulated biomass environment at 600 °C for 1000 h

potassium chloride is visible, followed by an incoherent mixed Ni/Cr-oxide, and a band of chromium depleted coating. Below this the remaining coating and substrate are unchanged.

The absence of an Al segregation layer in this kind of sample could be responsible for the differences in corrosion performance recorded for the different coatings. It has been reported in the literature [44] that Al could provide protection

Fig. 8 BSE cross-section image and EDX maps of NiCrAlY coated T92 exposed to a simulated biomass environment at 600 °C for 1000 h

from corrosion. It has also been noted that the appearance of depletion layers in NiCrAlY and A625 coatings, which show a different morphology respect to the rest of the coating, with the appearance of a what looks like increase in porosity/internal damage. This morphology is compatible with the "diffusion cell behaviour" reported by Evans [45].
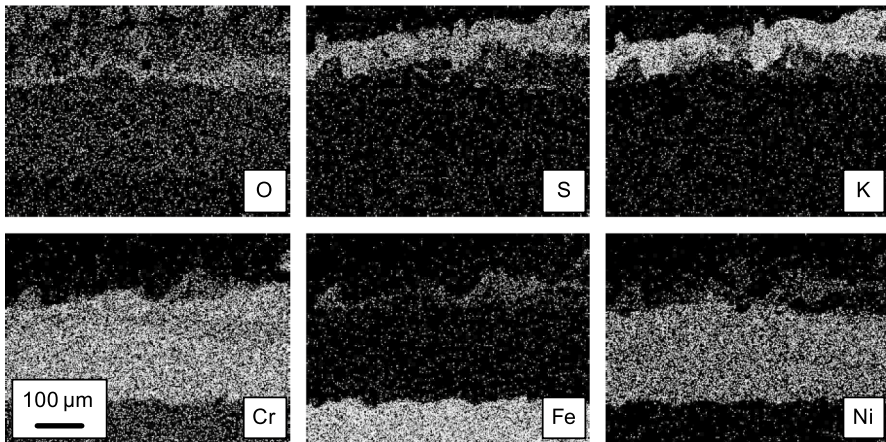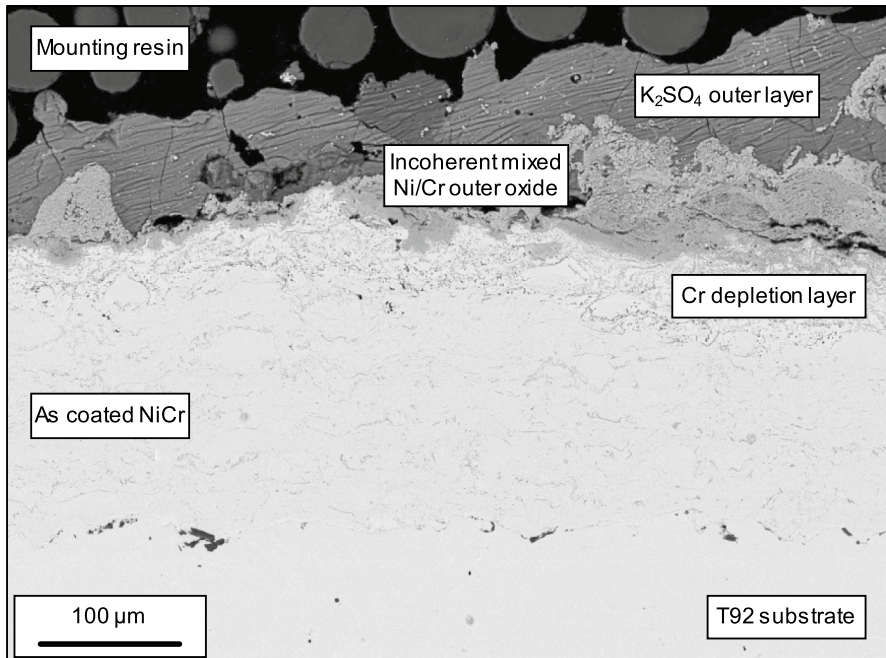
Fig. 9 BSE cross-section image and EDX maps of NiCr coated T92 exposed to a simulated biomass environment at 600 °C for 1000 h

Furthermore, the presence of a K-S rich layer has been reported, which is compatible with sulphidation of KCl from sulphur gaseous species present in the environment [46]. This sulphidation process could have led to a release of gaseous Cl or HCl to the environment, as per [46], which could be lost in the gas stream. This is in agreement with the EDX maps collected in this work, which don't show signs of Cl. Furthermore, has been reported the ability of KCl to dissolve Cr_2O_3 scale, and form

low melting point mixture with K_2CrO_4 or $K_2Cr_2O_7$ which could enhance the corrosion damage [47].

Conclusions

This study has investigated the fireside corrosion performance of candidate coatings for protecting superheater and reheater materials under biomass firing conditions. A typical alloy (T92) and four coating compositions (FeCrAl, NiCr, NiCrAlY and A625) applied by HVOF were exposed to laboratory simulated biomass combustion conditions at 600 °C for 1000 h with a potassium chloride deposit. The subsequent corrosion behaviour was assessed by weight change and dimensional metrology to determine the extent of any metal loss and internal damage. The results show that all but one of the coatings (HVOF NiCr) outperformed the T92 alloy. It was not possible to definitively conclude which coating composition provides the most protection since all samples showed signs of corrosion attack, highlighting the possibility of the formation of "diffusion cell". It has also highlighted the role of K and S in enhancing the corrosion damage. The first one (K) through its ability to form chromates and dissolving the chromia scale; while the second one (S) through the possibility of sulphidation reaction with KCl, which will then produce gaseous Cl or HCl.

Declarations

References

1. Roadmap 2050:*A Practical Guide to a Prosperous, Low-carbon Europe*. (European Climate Foundation, 2010).
2. J. Watson, R. Gross, I. Ketsopoulou, and M. Winskel, *Energy Policy* **87**, 685 (2015).
3. G. Camarsa, J. Toland, T. Hudson, S. Nottingham, W. Jones, J. Eldridge, et al. *LIFE and Climate change mitigation*. (European Union, 2015).
4. *A policy framework for climate and energy in the period from 2020 to 2030*. (European Commission, 2014).

5. A. Froggatt and A. Hadfield, *Deconstructing the European Energy Union: Governance and 2030 Goals*. (UK Energy Research Centre, 2015).
6. *State of play on the sustainability of solid and gaseous biomass used for electricity, heating and cooling in the EU*. (European Commission, 2014). https://doi.org/10.1017/CBO9781107415324.004.
7. M. Sami, K. Annamalai, and M. Wooldridge, *Progress in Energy and Combustion Science* **27**, 171 (2001). https://doi.org/10.1016/S0360-1285(00)00020-4.
8. A. H. M. Khodier, T. Hussain, N. J. Simms, J. E. Oakey, and P. J. Kilgallon, *Fuel* **101**, 53 (2012).
9. T. Hussain, A. H. M. Khodier, and N. J. Simms, *Fuel* **112**, 572 (2013).
10. A. Eisentraut and A. Brown, *International Energy Agency* 2012.
11. J. M. Cansino, M. Pablo-Romero, R. Román, and R. Yñiguez, *Energy Policy* **38**, 6000 (2010). https://doi.org/10.1016/j.enpol.2010.05.055.
12. N. Winchester and J. M. Reilly, *Energy Economics* **51**, 188 (2015). https://doi.org/10.1016/j.eneco.2015.06.016.
13. R. Saidur, E. A. Abdelaziz, A. Demirbas, M. S. Hossain, and S. Mekhilef, *Renewable and Sustainable Energy Reviews* **15**, 2262 (2011). https://doi.org/10.1016/j.rser.2011.02.015.
14. P. Thornley, *Energy Policy* **34**, 2087 (2006). https://doi.org/10.1016/j.enpol.2005.02.006.
15. M. Perry and F. Rosillo-Calle, *Biomass Bioenergy* **32**, 688 (2008). https://doi.org/10.1016/j.biombioe.2008.01.004.
16. B. M. Jenkins, L. L. Baxter, T. R. Miles, and T. R. Miles, *Fuel Processing Technology* **54**, 17 (1998). https://doi.org/10.1016/S0378-3820(97)00059-3.
17. A. Demirbas, *Progress in Energy and Combustion Science* **31**, 171 (2005). https://doi.org/10.1016/j.pecs.2005.02.002.
18. R. García, C. Pizarro, A. Álvarez, A. G. Lavín, and J. L. Bueno, *Fuel* **148**, 152 (2015). https://doi.org/10.1016/j.fuel.2015.01.079.
19. W. B. A. Sharp, *Superheater corrosion in biomass boilers: Today's science and technology (ORNL/TM-2011/399)*. (Oak Ridge National Laboratory, 2011).
20. H. P. Nielsen, F. J. Frandsen, and K. Dam-Johansen, *Energy and Fuels* **13**, 1114 (1999). https://doi.org/10.1021/ef990001g.
21. H. P. Nielsen, F. J. Frandsen, K. Dam-Johansen, and L. L. Baxter, *Progress in Energy and Combustion Science* **26**, 283 (2000). https://doi.org/10.1016/S0360-1285(00)00003-4.
22. F. J. Frandsen, *Fuel* **84**, 1277 (2005). https://doi.org/10.1016/j.fuel.2004.08.026.
23. Y. Shao, J. Wang, F. Preto, J. Zhu, and C. Xu, *Energies (Basel)* **5**, 5171 (2012). https://doi.org/10.3390/en5125171.
24. M. Montgomery, S. A. Jensen, U. Borg, O. Biede, and T. Vilhelmsen, *Materials and Corrosion* **62**, 593 (2011). https://doi.org/10.1002/maco.201005856.
25. T. Hussain, N. J. Simms, J. R. Nicholls, and J. E. Oakey, *Surface and Coatings Technology* **268**, 165 (2015). https://doi.org/10.1016/j.surfcoat.2015.01.074.
26. D. Fähsing, M. Rudolphi, L. Konrad, and M. C. Galetz, *Oxidation of Metals* **88**, 155 (2017). https://doi.org/10.1007/s11085-016-9684-2.
27. D. Wu, S. Liu, Z. Yuan, P. Cao, X. Wei, and C. Zhang, *Journal of Thermal Spray Technology* **30**, 1927 (2021). https://doi.org/10.1007/s11666-021-01248-1.
28. S. Mori, A. Pidcock, J. Sumner, N. J. Simms, J. E. Oakey, *Oxidation of Metals* n.d.
29. S. Mori, J. Sumner, J. Bouvet, N. J. Simms, *Materials at High Temperature* n.d.
30. N. Simms, M. Seraffon, A. Pidcock, and C. Davis, *Oxidation of Metals* **88**, 165 (2017). https://doi.org/10.1007/s11085-016-9680-6.
31. ASTM A213/A213M - *Standard Specification for Seamless Ferritic and Austenitic Alloy-Steel Boiler, Superheater, and Heat-Exchanger Tubes*. (ASTM International, 2015). https://doi.org/10.1520/A0213.
32. A. U. Syed, N. J. Simms, and J. E. Oakey, *Fuel* **101**, 62 (2012).
33. T. Hussain, N. J. Simms, and J. R. Nicholls, *Materials and Corrosion* **65**, 197 (2014). https://doi.org/10.1002/maco.201307063.
34. T. Hussain, A. U. Syed, and N. J. Simms, *Fuel* **113**, 787 (2013). https://doi.org/10.1016/j.fuel.2013.04.005.
35. N. J. Simms, A. T. Fry, *Technology (Singap World Sci)* 1192 (2012).
36. T. Hussain, A. U. Syed, and N. J. Simms, *Oxidation of Metals* **80**, 529 (2013). https://doi.org/10.1007/s11085-013-9394-y.

37. ISO—ISO 17224:2015—*Corrosion of metals and alloys—Test method for high temperature corrosion testing of metallic materials by application of a deposit of salt, ash, or other substances* n.d. https://www.iso.org/standard/59451.html (Accessed October 11, 2021).
38. J. R. Nicholls, N. J. Simms, and A. Encinas-Oropesa, *Materials at High Temperatures* **24**, 149 (2007). https://doi.org/10.3184/096034007X263587.
39. N. J. Simms, P. J. Kilgallon, and J. E. Oakey, *Materials at High Temperatures* **24**, 333 (2007). https://doi.org/10.3184/096034007X281640.
40. ISO—ISO 14802:2012—*Corrosion of metals and alloys—Guidelines for applying statistics to analysis of corrosion data* n.d. https://www.iso.org/standard/53991.html (Accessed October 11, 2021).
41. ISO—ISO 26146:2012—*Corrosion of metals and alloys—Method for metallographic examination of samples after exposure to high-temperature corrosive environments* n.d. https://www.iso.org/standard/54021.html (Accessed October 11, 2021).
42. A. Potter, J. Sumner, and N. J. Simms, *Materials at High Temperatures* **35**, 236 (2018). https://doi.org/10.1080/09603409.2017.1392413.
43. A. Zahs, M. Spiegel, and H. J. Grabke, *Corrosion Science* **42**, 1093 (2000). https://doi.org/10.1016/S0010-938X(99)00142-0.
44. M. Schütze, M. Malessa, V. Rohr, and T. Weber, *Surface and Coating Technology* **201**, 3872 (2006). https://doi.org/10.1016/j.surfcoat.2006.07.262.
45. H. E. Evans, M. P. Taylor, Oxidation of Metals 55 (2001). https://doi.org/10.1023/A:1010369024142.
46. P. J. James and L. W. Pinder, *Materials at High Temperatures* **14**, 187 (1997). https://doi.org/10.1080/09603409.1997.11689544.
47. T. M. Meißner, X. Montero, D. Fähsing, and M. C. Galetz, *Corrosion Science* **164**, 108343 (2020). https://doi.org/10.1016/j.corsci.2019.108343.

Authors and Affiliations

Andy Pidcock[1] · Stefano Mori[2] · Joy Sumner[2] · Nigel Simms[2] · John Nicholls[2] · John Oakey[2]

Joy Sumner
j.sumner@cranfield.ac.uk

Nigel Simms
n.j.simms@cranfield.ac.uk

John Nicholls
j.r.nicholls@cranfield.ac.uk

John Oakey
j.e.oakey@cranfield.ac.uk

[1] CorrosionRADAR, Cranfield, UK

[2] Cranfield University, College Road, Cranfield, Bedford MK43 0AL, UK